Isothermal Crystallization Kinetics of Sodium Dodecyl Sulfate–Water Micellar Solutions

Ruhina M. Miller[†,‡], Andreas S. Poulos[‡], Eric S. J. Robles[§], Nicholas J. Brooks[†], Oscar Ces[†], João T. Cabral[‡]*

[†]Department of Chemistry and Institute of Chemical Biology, Imperial College London, London SW7 2AZ, United Kingdom

[‡]Department of Chemical Engineering, Imperial College London, London SW7 2AZ, United Kingdom

[§]The Procter & Gamble Company, Newcastle Innovation Centre, Newcastle-Upon-Tyne NE12 9TS, United Kingdom

The crystallization mechanisms and kinetics of micellar sodium dodecyl sulfate (SDS) solutions in water, under isothermal conditions, were investigated experimentally by a combination of reflection optical microscopy (OM), differential scanning calorimetry (DSC) and attenuated total reflection Fourier transform infrared spectroscopy (ATR-FTIR). The rates of nucleation and growth were estimated from OM and DSC across temperatures ranging from 20 to -6 °C for 20% SDS-H_2O, as well as for 10 and 30% SDS-H_2O at representative temperatures of 6, 2 and -2 °C. A decrease in temperature increased both nucleation and growth rates, and the combined effect of the two processes on the morphology was quantified via both OM and ATR-FTIR. Needles, corresponding to the hemihydrate polymorph, become the dominant crystal form at ≤-2 °C, while platelets, the monohydrate, predominate at higher temperatures. Above 8 °C, crystallization was only observed if seeded from crystals generated at lower temperatures. Our results provide quantitative and morphological insight into the crystallization of ubiquitous micellar SDS solutions and its phase stability below room temperature.

* João T. Cabral
Department of Chemical Engineering
Imperial College London
London SW7 2AZ
United Kingdom
+44(0)20 7594 5571
j.cabral@imperial.ac.uk

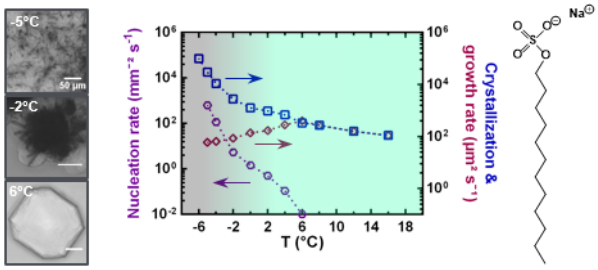

Isothermal Crystallization Kinetics of Sodium Dodecyl Sulfate–Water Micellar Solutions

Ruhina M. Miller[†,‡], Andreas S. Poulos[‡], Eric S. J. Robles[§], Nicholas J. Brooks[†], Oscar Ces[†], João T. Cabral[‡]*

[†]Department of Chemistry and Institute of Chemical Biology, Imperial College London, London SW7 2AZ, United Kingdom

[‡]Department of Chemical Engineering, Imperial College London, London SW7 2AZ, United Kingdom

[§]The Procter & Gamble Company, Newcastle Innovation Centre, Newcastle-Upon-Tyne NE12 9TS, United Kingdom

Keywords: Surfactants, sodium dodecyl sulfate, crystallization, nucleation, growth

ABSTRACT: The crystallization mechanisms and kinetics of micellar sodium dodecyl sulfate (SDS) solutions in water, under isothermal conditions, were investigated experimentally by a combination of reflection optical microscopy (OM), differential scanning calorimetry (DSC) and attenuated total reflection Fourier transform infrared spectroscopy (ATR-FTIR). The rates of nucleation and growth were estimated from OM and DSC across temperatures ranging from 20 to -6 °C for 20% SDS-H_2O, as well as for 10 and 30% SDS-H_2O at representative temperatures of 6, 2 and -2 °C. A decrease in temperature increased both nucleation and growth rates, and the combined effect of the two processes on the morphology was quantified via both OM and ATR-FTIR. Needles, corresponding to the hemihydrate polymorph, become the dominant crystal form at ≤-2 °C, while platelets, the monohydrate, predominate at higher temperatures. Above 8 °C, crystallization was only observed if seeded from crystals generated at lower temperatures. Our results

provide quantitative and morphological insight into the crystallization of ubiquitous micellar SDS solutions and its phase stability below room temperature.

INTRODUCTION

Surfactants, or surface active agents, are amphiphilic molecules used in a variety of industries, including personal care and household, pharmaceuticals, agriculture and food.[1,2] Surfactants can considerably reduce the interfacial tension between immiscible fluids,[3,4] and can increase the stability of everyday products, for example detergents[5,6] and emulsions,[7–9] from milliseconds to months or years.[8,10] Sodium dodecyl sulfate (SDS), also known as sodium lauryl sulfate (SLS) is an anionic, alkyl sulfate surfactant widely used in industry and academia; it is employed in applications ranging from formulations such as shampoos[2] to DNA separation.[11] The phase diagram for the binary SDS-H_2O system is well-established,[12–14] shown in Figure 1.

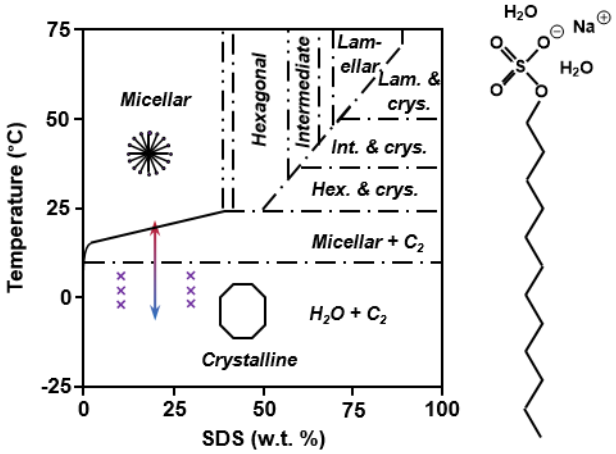

Figure 1. Simplified SDS-H_2O phase diagram (adapted from[12,14]) and a skeletal drawing of a hydrated SDS molecule. The arrow and crosses denote the SDS-H_2O concentrations (10, 20 and 30%) and temperature range (-6 to 22 °C) investigated.

For a crystalline dispersion the polymorph, morphologies and size distributions of the crystals has profound processing and performance implications,[15–17] including: how the material flows and settles[18] its rate of dissolution,[19] optical appearance, texture and rheology.[10] Needle-shaped crystals, for instance, are often undesirable during processing due to their high aspect ratio.[16] The crystal habit is affected by a range of

factors influencing nucleation and growth:[20–24] temperature, concentration, pH, volume,[25,26] rate of cooling,[10] additives,[27] impurities and other factors. Surfactant formulations are often subject to temperature variations during manufacture, storage, transportation[1,10,28] and use.[18] Minimizing impurities is also a consideration as it can impact transition temperatures,[12] crystal habit[21,23,29] and metastable zone widths (MSZWs),[22] due to integration into the crystal lattice. SDS undergoes an autocatalytic, acid-catalyzed hydrolysis reaction that produces 1-dodecanol and hydrogen sulfate, the rate dependent on concentration, temperature and pH.[30,31]

SDS is a highly soluble surfactant,[32] forming different phases, including hydrated crystals, depending on the concentration and temperature. These can interconvert according to their thermodynamic stability in a given region.[20,29,33,34] Polymorphs, including pseudopolymorphs, exhibit distinct physical properties;[16,34,35] this is well-studied for pharmaceutical systems[23,36] and can also be important for surfactant crystallization. Five hydration states have been reported for SDS-H_2O crystals: ⅛ hydrate,[37] hemihydrate,[38] monohydrate,[39] dihydrate[12] and anhydrous.[40] The ⅛ hydrate has a monoclinic *C2/c* structure;[37] a similar form was previously identified as a monoclinic *Aa* or *A2/a* structure[41,42] (a non-standard setting of *Cc* or *C2/c*, space group numbers 9 and 15 respectively). The hemihydrate, monohydrate and anhydrous phases have a monoclinic *C2*,[38] triclinic $P\bar{1}$[39] and monoclinic $P2_1/c$[40] structure respectively. The crystal phases have also been investigated by Raman and FTIR spectroscopy.[43–45] DSC,[12] X-ray, NMR and optical microscopy[13] was used to establish the equilibrium phase diagram for SDS-H_2O. From optical microscopy[46] and turbidimetry,[47] the impact of cooling rate ($\leq$0.75 °C min^{-1}) on the crystalline transition temperatures, MSZW and saturation of SDS-H_2O micellar solutions was found to be marginal. Platelets were observed >0 °C[46] and the crystal structure was modelled computationally.[46,48]

Although the crystallization of SDS from solution has been examined for several decades,[12,13,37–48] an unequivocal correspondence between crystallization kinetics, morphology and polymorphs under isothermal conditions is lacking. This paper seeks to understand and quantify the rates of nucleation, overall crystallization kinetics and morphologies of SDS-H_2O micellar solutions (rapidly) quenched and held isothermally below the crystallization phase boundary. A wide range of temperatures, from 20 to -6 °C was

investigated, over which the interplay between nucleation and growth is examined, and the non-equilibrium crystal habits and structures identified.

EXPERIMENTAL SECTION

Materials

SDS (ACS reagent grade, ≥99.0% purity) was purchased from Sigma Aldrich and used as received; a very high purity grade was chosen for the reasons outlined above. Deionized water was obtained from a Centra ELGA filtration system. SDS-H_2O compositions in the micellar region: 10, 20 and 30% were prepared by weight percentage, sonicated for 20 min and were left for at least 24 h at 22 °C (for 10, 20%) and 28 °C (30%) to allow for equilibration. To maintain consistency factors such as pH ≈ 7 and indications of hydrolysis were monitored, the latter via ^1H nuclear magnetic resonance (NMR) spectroscopy. Further details of the NMR studies and reported peaks are provided in the Supporting Information (Figure S1).

The SDS-H_2O solutions were filtered through a 0.2 μm PTFE syringe filter and were loaded into flat, rectangular capillary tubes (CM Scientific, cross-section 50 x 500 μm^2). These were sealed with an epoxy-based adhesive (Araldite Rapid) and were left overnight. New capillaries were prepared for every experiment to keep seed crystals to a minimum and to maintain a homogenous solution, as repeated heating and cooling can introduce concentration discrepancies. Capillaries were employed to keep impurities to a minimum, as complete removal is challenging[25,49] and because temperature equilibration is faster at these small length scales.

Optical microscopy

Optical microscopy was carried out with an Olympus BX41M-LED reflection microscope, equipped with a 10x objective and a CCD camera (Allied Vision, Prosilica GX 1050C). The images were analyzed with ImageJ 1.48v (NIH); the procedure is detailed in the Supporting Information (Figure S2).

The temperature was regulated using a Linkam Scientific THMS600 temperature controlled stage, which has ±0.1 °C accuracy and stability. Prior to each experiment, samples were equilibrated to ensure that the solution was fully micellar, as described above. Isothermal crystallization experiments were conducted by rapidly cooling the sample to the desired temperature at a rate of 50 °C min^{-1}. For the temperature range investigated, 20 to -6 °C, the cooling stage takes between 2 and 34 s to reach the target temperature; time zero, $t = 0$, is defined as when this was reached. The isothermal temperatures investigated were: 20, 16, 12, 10, 8, 6, 4, 2, 0, -2, -4, -5 and -6 °C, observation times ranging from 0 to 21500 s, depending on crystallization kinetics, and typically four repetitions per data point.

Differential scanning calorimetry (DSC)

DSC was conducted using a TA Instruments Q2000 DSC, which has ±0.1 °C accuracy, calibrated with indium. Samples (≈15 mg) were freshly prepared in aluminum hermetic pans (Tzero) and were weighed before and after each experiment to ensure that no mass loss had occurred. The following temperature profile was employed: the sample was held at 30 °C for 60 s, then cooled at 10 °C min^{-1} to the desired hold temperature: 6, 4, 2, 0, -1 or -2 °C, with a minimum of two repetitions per experiment. Faster cooling rates resulted in lower quality data and were thus not employed. Approaching the set temperature, the equipment cools at approximately 3 °C min^{-1}, introducing a small stabilization window, t_{stabil}, duration between 16 to 45 s depending on the final temperature. Data extraction was carried out with the TA Instruments Universal Analysis 2000 software.

Attenuated total reflection Fourier transform infrared spectroscopy (ATR-FTIR)

ATR-FTIR spectra were measured using a Bruker Tensor 27 System with a Platinum ATR accessory. Parameters were set to 4 cm^{-1} resolution, 4000 to 600 cm^{-1}, single beam and absorbance mode. Crystalline material was grown in glass capillaries (4.2 mm diameter) by cooling at 50 °C min^{-1}; a portion extracted and examined with reflection optical microscopy to establish the morphology and quality of the crystals before

conducting the ATR-FTIR measurements, cooled by an external unit. ATR-FTIR enabled determination of the crystalline hydration states; additionally the micellar solution was run as a reference point. Results were collected and examined using OPUS 6.5.

RESULTS AND DISCUSSION

Analysis procedure

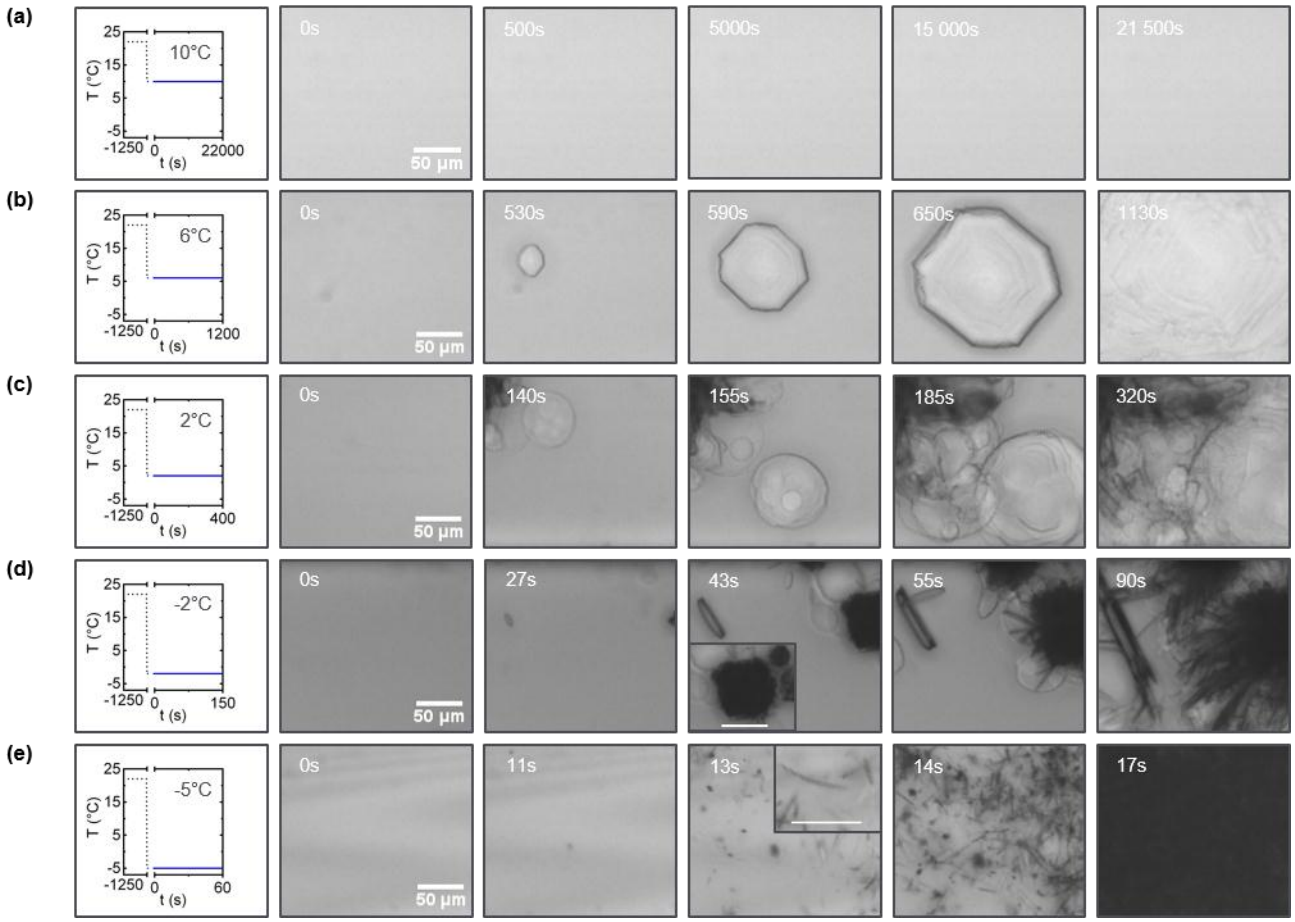

Figure 2. Optical microscopy images of 20% SDS-H_2O solutions showing the development of crystal nucleation and growth at various temperatures; the implemented thermal profile is shown on the left panels. (a) 10 °C. (b) 6 °C. (c) 2 °C. (d) -2 °C. (e) -5 °C. The solutions were equilibrated for 20 min, rapidly cooled at 50 °C min^{-1} to the desired temperature and held isothermally for the relevant time interval.

For every temperature, crystal nucleation and growth parameters were estimated using reflection optical microscopy from $t = 0$ until the solution was saturated, the finish time (t_f), defined as when no further crystallization was observed (≤6 h). Figure 2 depicts the evolution of representative crystal habits over time, at selected temperatures. The number density of nuclei and the crystalline area fraction were determined from a representative 0.2 mm² area. Experimental uncertainties were estimated from four repetitions with distinct samples. Relevant nucleation and growth rates were calculated for each acquisition, and the final value shown is the average, while the error is the maximum deviation between the datasets and the reported average.

Illustrative results for the solutions at -5 °C are shown in Figure 3. The number (area) density of nuclei (mm^{-2}), Figure 3(a) and the crystal area fraction, Figure 3(c) both increase over time with a sigmoidal profile, characteristic of crystallization.[50] The parameters extracted include the final crystal number density N_∞, the induction time t_{ind}, the completion time $t_{f(N)}$, and the duration of the nucleation process, $\Delta t_{(N)} = t_{f(N)} - t_{ind}$. The derivative of N_d with time has a reasonable fit to a Gaussian curve, shown in Figure 3(b). From this the maximum rate of nucleation $(dN_d/dt)_{max}$ and the overall rate, $N_\infty/\Delta t_{(N)}$ can be estimated. The same procedure was followed for the area fraction A_f and its derivative, Figures 3(c) and (d); areas (A) were normalized to the value corresponding to the representative area (0.2 mm^2) being fully crystalline (ΣA), $A_f = A/\Sigma A$. From this t_f, Δt and the half-time for crystallization $t_{1/2}$, defined as the time corresponding to A_f reaching 50%,[51] and the maximum and overall crystallization rates: $(dA/dt)_{max}$ and $\Delta A/\Delta t$ respectively were obtained. Growth rates of isolated, single, crystals were also computed in terms of the evolution of the crystal area over time, whose maximum value is reported $(dG/dt)_{max}$. A more detailed analysis in terms of both crystals lengths and area is presented in Supporting Information (Figure S5, S6). In Whilst optical microscopy is an effective tool to analyze crystal morphologies and mechanisms,[16] its limited spatial resolution (≈4 μm² for this magnification) exceeds the dimensions of the critical nucleus, r_c; t_{ind} is thus an upper limit.

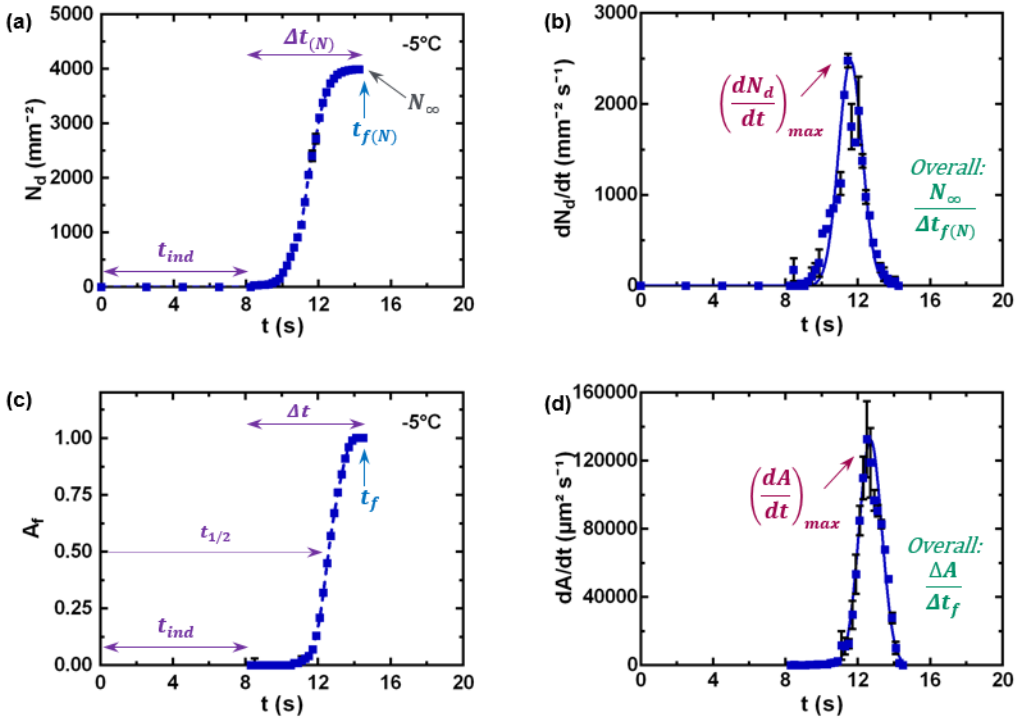

Figure 3. Representative analysis of the optical microscopy images for 20% SDS-H_2O solutions; graphs are as a function of time. Solutions were held isothermally at -5 °C after a rapid cooling quench from the micellar phase, shown in Figure 2(e). (a) Crystal number (area) density (N_d). (b) Rate of nucleation (dN_d/dt). (c) Normalized change in crystalline area A_f *(= A/ΣA)*. (d) Crystallization rate (dA/dt). The dotted lines serve as a guide to the eye and the solid lines are Gaussian fits; the remaining parameters are described in the text.

Nucleation kinetics

The compilation of experimental data for nucleation at various temperatures is shown in Figure 4. As seen in Figure 2, nucleation densities vary widely across the temperature range. N_d is thus normalized by its final value to give a nucleation fraction, $N_f = N_d/N_\infty$, data in Figure 4(a); the absolute N_d data is provided in the Supporting Information (Figure S3). Nucleation becomes more favorable and the kinetics increase with supersaturation and lowering solubility, namely with decreasing temperature.[23] $(dN_d/dt)_{max}$ and N_∞ thus decrease exponentially with temperature, varying by up to five orders of magnitude, as shown in Figure 4(b).

It has been suggested that at high levels of supersaturation, the energy barrier for nucleation is significantly lower, such that crystallization occurs in the spinodal regime.[24]

Nucleation was observed at all temperatures <6 °C, therefore this was identified as the labile region.[20,29] Above 6 °C, nucleation was not observed within 6 h following an isothermal quench, therefore this is the metastable[33,52] region, shaded blue in Figure 4(b). In this window nucleation is possible but not certain, and is expected to occur over long timescales.[20]

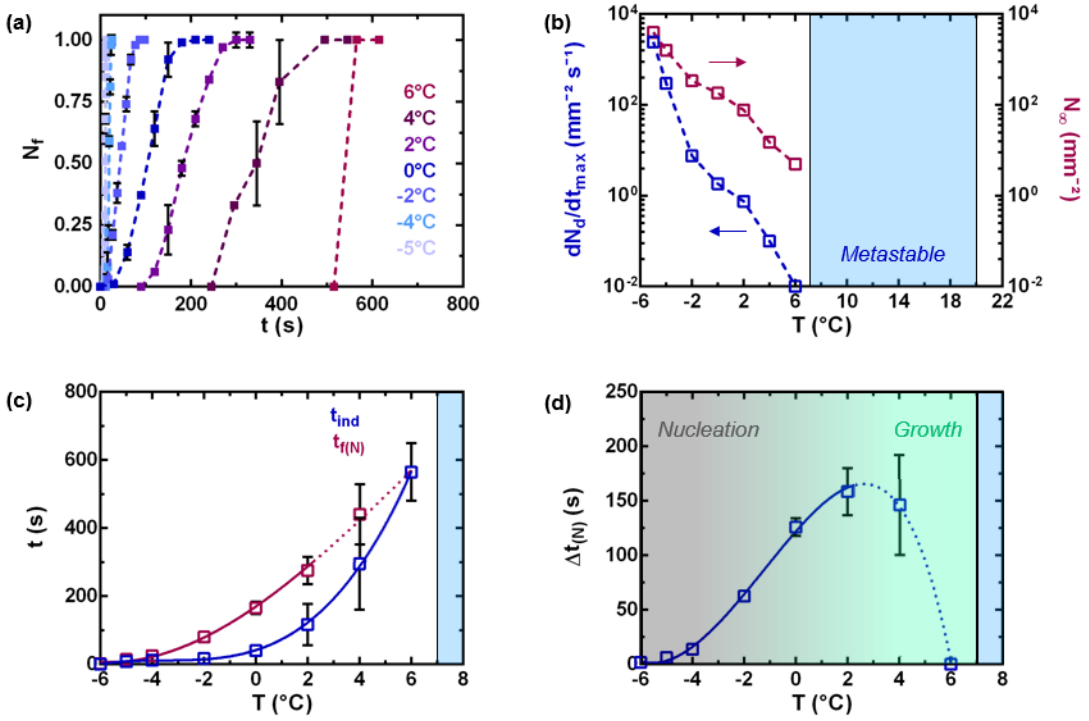

Figure 4. Nucleation parameters for 20% SDS-H_2O solutions held isothermally after a cooling quench to the temperatures indicated. (a) Normalized number density (N_f) of crystals as a function of time. (b) Rate of nucleation ($(dN_d/dt)_{max}$ – dark blue, left axis) and total number density (N_∞ – dark red, right axis) as a function of temperature; the region >6 °C is termed supercooled as nucleation was not observed ≤6 h. (c) Induction (t_{ind}) and finish ($t_{f(N)}$) times for nucleation. (d) Nucleation duration, $\Delta t_{(N)} = t_{f(N)} - t_{ind}$; the non-monotonic evolution of $\Delta t_{(N)}$ relates to the cross-over to a growth-dominated regime.

Lower temperatures yield shorter characteristic timescales, shown in Figure 4(c), with t_{ind} reaching 7.8 ± 0.9 s by -5 °C. Consequently $t_{f(N)}$ also decreases with temperature as the process begins earlier, for instance $t_{f(N)}$ is 14 ± 2 s at -5 °C, with $\Delta t_{(N)}$ at 6.4 ± 0.6 s. Below -5 °C instantaneous nucleation transpires as almost all of the crystals nucleate at once [53] due to high saturation and very low solubility; above this temperature progressive nucleation occurs. It is considered, however, that whilst temperature equilibration is rapid at these length scales, analysis at temperatures ≥-4 °C is challenging as t_{ind} becomes commensurate with the cooling time. With increasing temperature t_{ind} increases exponentially, reaching 565 ± 85 s by 6 °C, Figure 4(c). $\Delta t_{(N)}$ initially increases, however after 2 °C it begins to decrease and by 6 °C $\Delta t_{(N)} \approx 0$. The convergence of t_{ind} and $t_{f(N)}$, which results in $\Delta t_{(N)}$ tending to 0 is due to growth, as opposed to nucleation being the governing factor; one crystal thus forms within the representative area by 6 °C. The curve for this region in Figures 4(c) and (d) have therefore been dashed. The maximum $\Delta t_{(N)}$ at 2 °C $\approx$ 160 ± 20 s thus delimits the nucleation and growth dominated regions. At both ends of the temperature scale well-defined habits are observed: a large number of crystals with a narrow size distribution at low temperatures (≤-4 °C), where nucleation dominates, and one to several large crystals at high temperatures (≥2 °C) where growth dominates. At even higher temperatures, >6 °C, nucleation events become extremely sporadic (>6 h); this range is essentially supercooled.

Classical nucleation theory[29,54] provides a simple but useful framework to rationalize the nucleation process. At high supersaturation, localized concentration fluctuations result in the transient formation of nuclei as ordered molecules. Clusters with dimensions below r_c dissolve back into the liquor, whereas larger ones grow.[55] Whilst the micellar solutions comprise predominantly of micelles, the reported SDS crystal structures adopt lamellar structures.[37–40] This system may therefore proceed via a more complex, two-step mechanism: in a supersaturated solution, disordered clusters or aggregates, termed precursors, may form in dense regions of higher supersaturation. These can combine, and undergo rearrangements to yield ordered phases characteristic of the final crystalline structure, which then proceed into the growth phase.[54]

Crystallization kinetics – Optical microscopy

Crystal growth analysis was conducted on isolated crystals and in terms of an overall crystallized area fraction. Crystallization often yields a size distribution of crystals, and crystal growth is eventually affected by the density of neighboring crystals, solute depletion and finite sample volume.[22,24] The combination of single crystal and ensemble analysis allows for extraction of the overall crystallization kinetics within the sample volume, as well as morphological characterization.

The change in crystalline area over time, for each temperature, was estimated by optical microscopy and is shown in Figure 5(a) as an area fraction, A_f. For the early stages of crystallization in particular, these values are generally larger than the corresponding crystalline volume fractions as surfactants tend to grow as thin needles and platelets.[45] The data displays the same characteristic sigmoidal profiles as N_f in Figure 4(a), becoming increasingly stretched in time at higher temperatures as the nucleation rate is slower, thus isolated crystals grow larger. Above 6 °C nucleation was not observed ≤6 h, as shown in Figure 4(b), which is below the crystallization phase boundary of ≈ 20 to 21 °C for this composition. Crystals are found to grow in this region if a seed crystal, generated at a lower temperature, is used. In order to evaluate the growth rates within the temperature range of 8 to 20 °C, samples were first cooled to 6 °C for approximately 10 min to generate this seed crystal; before rapidly heating the solution (at 50 °C min^{-1}) to the desired temperature. Varying seeding time and temperature did not significantly affect the crystallization rate estimates, within measurement uncertainty, Supporting Information (Figure S4). Seeded growth experiments were conducted at 8, 12, 16, and 20 °C, with the data shown in Figure 5(b). Growth was not observed for the last temperature and nucleation was not observed at any temperature within this range.

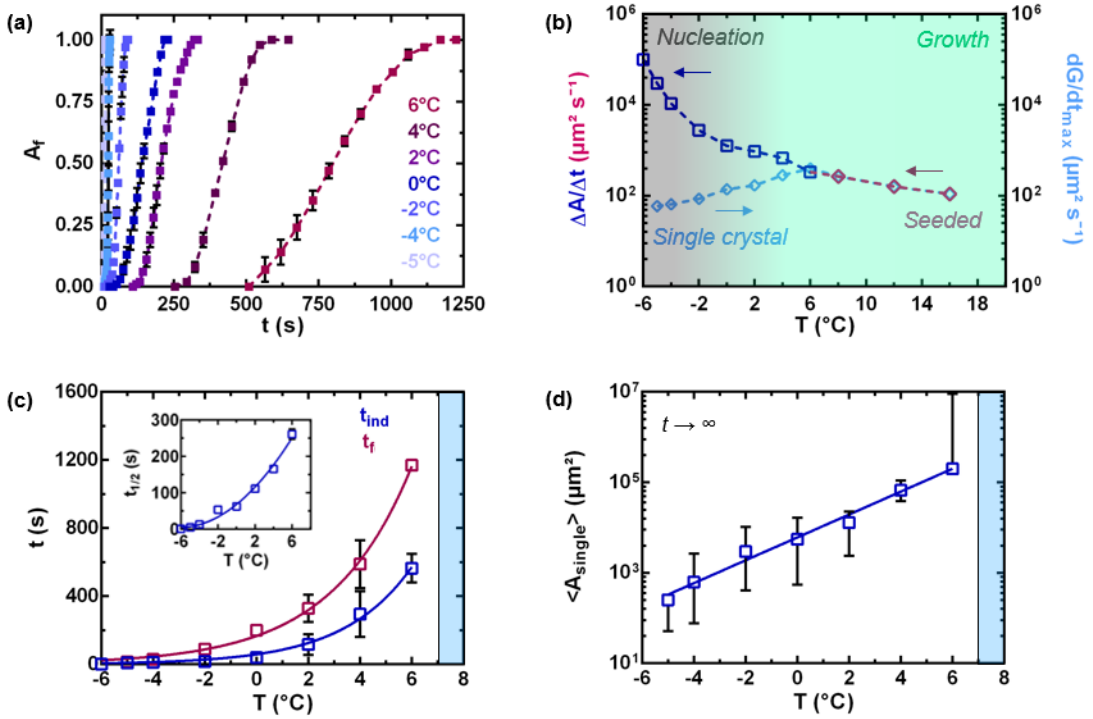

Figure 5. Crystallization data for 20% SDS-H_2O solutions held isothermally after a cooling quench to the temperatures indicated. (a) Evolution of A_f with time. (b) Overall rate of crystallization ($\Delta A/\Delta t$), including the temperature range >6 °C where the solutions were seeded. The grey and green regions denote where nucleation and growth, respectively, are more favorable. (c) Induction (t_{ind}) and finish (t_f) times for growth. Inset: crystallization half-time ($t_{1/2}$). (d) Average crystal size ($<A_{single}>$), estimated by $\Sigma A/N_\infty$.

The overall crystallization rate $\Delta A/\Delta t$, shown in Figure 5(b), decreases with increasing temperature predominantly due to lower nucleation rates. Between -6 and -4 °C there is a sharp increase in crystallization rates, with $\Delta A/\Delta t$ reaching $(30 \pm 1)\cdot 10^3$ μm² s^{-1} by -5 °C, as the nucleation rate is high. Crystals (needles) grow rapidly along the fastest faces but remain relatively small due to the high N_∞, consequently restricting growth and resulting in a narrow size distribution. At the other end of the temperature scale, low crystallization rates, around 110 ± 15 μm² s^{-1} for $\Delta A/\Delta t$ at 16 °C, are found when growth, as opposed to nucleation, dominates. By the highest unseeded range, between 2 and 6 °C, the low N_∞ enables crystals to grow much larger before encountering another crystal, with growth the governing process. Above 6 °C

nucleation is extremely low; the crystallization rate in this case was thus determined by analyzing the growth of seed crystals.

With increasing temperature t_f and t_{ind} increase exponentially, given in Figure 5(c); by 6 °C t_f is 1170 ± 30 s. In turn this is reflected in Δt, which is 31 ± 4 min at 16 °C compared to 6.7 ± 0.3 s at -5 °C. The *average* single crystal area $\langle A_{single} \rangle = \Sigma A / N_\infty$, shown in Figure 5(d), is calculated from the nucleation density and the overall crystallized area. As the temperature is lowered N_∞ increases, therefore $\langle A_{single} \rangle$ decreases, as there is a trade-off between nucleation and growth due to solute limitations.[23] Crystal growth analysis was also evaluated directly on individual, isolated, crystals, and is reported in Supporting (Figure S5, S6). Four to eight representative crystals were examined for each morphology, per temperature. Due to size polydispersity as the nucleation rate decreases, we opt to focus on we opt to focus on the crystalline area A (or A_f). In general, needle-shaped crystals were found to grow slower than platelets at the same temperature when examining $(dArea/dt)_{max}$, as illustrated in Supporting Information (Figure S6). While the rate of the fastest growing face of needles is higher, their growth is predominantly uniaxial; by contrast, platelets grow along a plane and therefore, their single crystal growth rate $(dG/dt)_{max}$ by area is higher. As shown in Figure 5(b), the single crystal growth rate is thus non-monotonic with temperature, increasing from low temperatures as needles give way to platelets, and then decreasing again at higher temperatures (>6 °C), within the seeded, single platelet range, towards the phase boundary.

The cross-over between nucleation-dominated and growth-dominated regimes is estimated to occur around 4-6 °C, by the coincidence of a number of observations. At these temperatures, the nucleation rate drops below $(dN_d/dt)_{max} \approx 0.1$ $mm^{-2}s^{-1}$, as shown in Figure 4(b). Further, the nucleation duration, $\Delta t_{(N)}$, shown in Figure 4(d), decreases as growth becomes prevalent. Finally, the growth rate approaches a maximum $(dG/dt)_{max} \approx 350 \pm 50$ $\mu m^{-2}s^{-1}$, related to the lower single crystal growth rate of needles compared to that of platelets, in area terms.

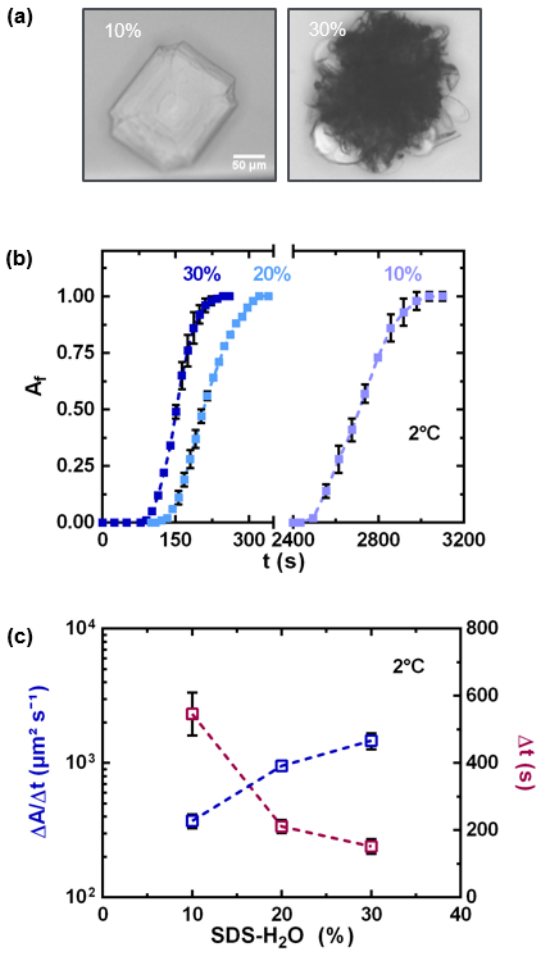

Figure 6. Effects of SDS concentration on the crystallization kinetics for three SDS-H_2O micellar concentrations: 10, 20 and 30%, held isothermally at 2 °C. (a) Optical microscopy images of the predominant crystal habit of 10 and 30% SDS-H_2O solutions. (b) Evolution of the crystal area fraction (A_f) with time. (c) Overall rate of crystallization ($\Delta A/\Delta t$ – dark blue, left axis) and duration of crystallization (Δt – dark red, right axis) as a function of concentration.

Additional concentrations of 10 and 30% SDS-H_2O, both within the micellar region, were examined to evaluate the generality of the findings. Representative crystals are shown in Figure 6(a), with the data in Figures 6(b) and (c) for a fixed temperature of 2 °C, extracted from optical microscopy images (and additional temperatures are provided in Supporting Information Figure S7). Qualitatively, the observed habits at 10% SDS-H_2O, 2 °C and 20% SDS-H_2O, 6 °C are similar, corroborated by the numerical estimates: on

average $\Delta A/\Delta t \approx 350 \pm 20\ \mu m^2\ s^{-1}$ and $\Delta t \approx 575 \pm 30$ s. For 30% SDS-H_2O at 2 °C, the habits observed were comparable to 20% at -2 °C. Further, the morphologies of (10% SDS, -2 °C), (20% SDS, 2 °C) and (30% SDS, 6 °C) are all qualitatively similar. An approximate shift of 3 to 4°C per 10% of added SDS seems to apply to all crystallization morphologies within the experimental window investigated. As expected, with decreasing SDS content the crystallization rate decreases and t_{ind} increases (considerably), as there is a lower solute concentration available for nucleation and growth. Overall the results indicate that the conclusions obtained from 20% SDS-H_2O can be extended to other micellar concentrations, with the appropriate kinetic shift depicted in Figure 6(c).

Crystallization kinetics – DSC

DSC provides complementary information to the optical microscopy study, quantifying the crystallization exotherms and providing further insight into crystallization kinetics. The thermal profile described above was employed, resulting in a stabilization time, t_{stabil}, before the sample reaches the desired isothermal temperature. Temperatures below -2 °C could thus not be recorded, as t_{stabil} becomes commensurate with t_{ind}.

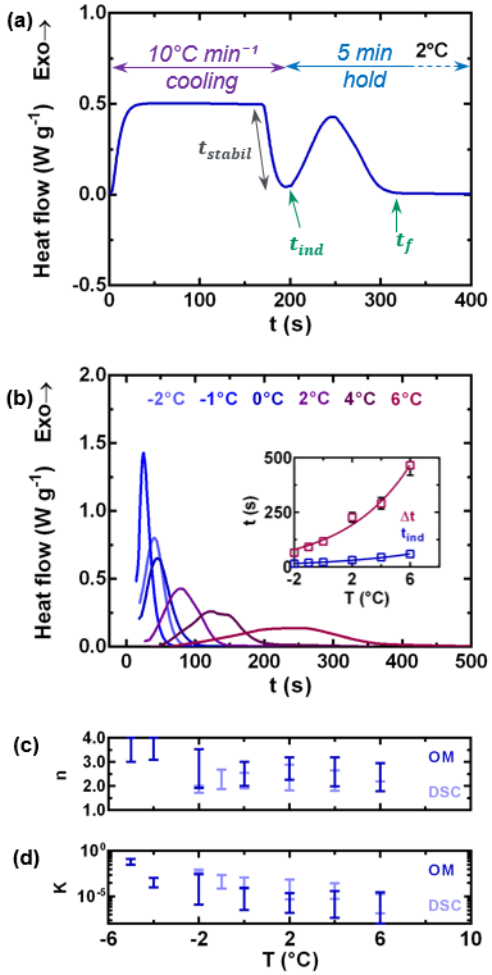

Figure 7. DSC data for solutions held isothermally following a cooling quench from the micellar phase and the Kolmogorov–Johnson–Mehl-Avrami (KJMA) parameters for all of the crystallization data. (a) Representative analysis for solutions at 2 °C. (b) DSC traces of heat flow from when the target temperature was reached against time. Inset: induction (t_{ind}) and duration (Δt) times. (c) and (d) KJMAs parameter n and K respectively for DSC (dark blue) and optical microscopy (light blue).

A representative DSC trace for 20% SDS-H_2O at 2 °C is shown in Figure 7(a), with the traces for each temperature, from when the set temperature was reached (after t_{stab}), in Figure 7(b). The full profiles, including the cooling ramp, are shown in Supporting Information (Figure S8). With increasing temperature t_{ind} and Δt increase, shown in the inset of Figure 7(b), which is in good agreement with the optical microscopy data. Rate constants were extracted by determining the relative degree of crystallinity, using:

$$\alpha(t) = \frac{\int_{t_{ind}}^{t} \frac{dH_C}{dt} dt}{\int_{t_{ind}}^{t_f} \frac{dH_C}{dt} dt} \quad (1)$$

where dH_C/dt is the heat flow,[56–58] yielding normalized values between 0 and 1. The average enthalpy of crystallization was estimated as 21.5 ± 3.3 kJ g^{-1} across the temperatures. The value was found to increase with temperature, specifically as the ratio of platelets (the monohydrate polymorph) increased, discussed later. As the crystal structures of this surfactant are composed of ≥88% SDS (with the structures observed >94% SDS)[12] the molar enthalpy was referenced to the latter SDS content, thus calculated to be 5.8 ± 0.9 kJ mol^{-1}.

Avrami kinetic analysis – Optical microscopy and DSC

Both the optical microscopy and DSC data were fitted to the descriptive Kolmogorov–Johnson–Mehl-Avrami equation (KJMA or 'Avrami' equation) [50,59,60]:

$$\alpha(t) = 1 - exp(-K(t-t_{ind})^n) \quad (2)$$

where $\alpha(t)$ is the crystalline volume fraction, K (s^{-n}) the rate constant for crystallization and $n = n_d + n_t$, where n_d is the dimensionality of growth, with a value between 1 and 3, and n_t is the time dependence of nucleation, ranging from 0 for instantaneous growth to 1 for sporadic growth.[61] Typically n_d is expected to be 1 for rod-like crystals, 2 for discs and platelets and 3 for spheres.[59,60] Equation (2) can also be written in the form $\alpha(t) = 1 - exp(-[k(t-t_{ind})]^n)$,[62] ensuring the rate units for k (s^{-1}).

A nonlinear least squares fit[63] was used to estimate the Avrami parameter K and exponent n, the results of which are shown in Figures 7(c) and (d). For both measurements K decreases exponentially with increasing temperature, as the crystallization rate decreases. The exponent n has an inherently large uncertainty across the temperature range studied. For DSC $n \approx 2.3$, the value of which is compatible with the relatively two-dimensional morphologies observed via microscopy, as surfactants crystallize as thin needles and platelets.[45] The value of n estimated from optical microscopy is higher at $n \approx 2.9$; this is likely due to the assumption that

the area and volume fractions can be equated. In turn, a higher value of n yields a (trivially) lower value of K, as expected from equation (2).

Parameter K can be described by an Arrhenius temperature dependence, whose activation energy is calculated from $ln\ k = ln\ A\ exp(-E_a/RT)$, where $k = K^{1/n}$ (s^{-1}),[64] A (s^{-1}) is the pre-exponential factor, and R (kJ K^{-1} mol^{-1}) the ideal gas constant. From the optical microscopy and DSC data, $E_a \approx 218 \pm 46$ kJ mol^{-1}.

The timescales for crystallization appear shorter with the DSC experiments compared to optical microscopy. This difference is rationalized terms of the larger volumes of the DSC samples (≈15 mm^3) compared to the capillaries (≈0.5 mm^3) employed in the optical microscopy experiments. Heterogeneous nucleation, particularly important at higher temperatures, is expected to scale with sample volume, extensively reported for aqueous systems.[25,26] Control experiments using optical microscopy experiments with varying capillary volumes revealed a slight decrease of t_{ind} with increasing volume. The lower cooling rate for the DSC studies, during t_{stab} in particular, is expected to have the most impact as the solution spends longer in the labile region whilst cooling. This was also tested via optical microscopy, with rates ≤10 °C min^{-1} exhibiting nuclei between 6 and -2 °C.

Morphology and other analysis

Surfactants generally crystallize with morphologies that have a high surface area to volume ratio, such as needles and platelets,[45] both exclusively noted in this study. Here the needles are further categorized as bundles or single needles. Figure 8(a) shows the representative crystal habits observed at various temperatures, and Figures 8(b)(i) and (ii) give the proportion of each morphology for the unseeded temperatures (≤6 °C). An example of the analysis is provided in the Supporting Information (Figure S9(a)) for the -5 °C solutions. Overall at high temperatures (≥6 °C) platelets are exclusively observed, however as the temperature is decreased the proportion of needles increases over a relatively narrow window.

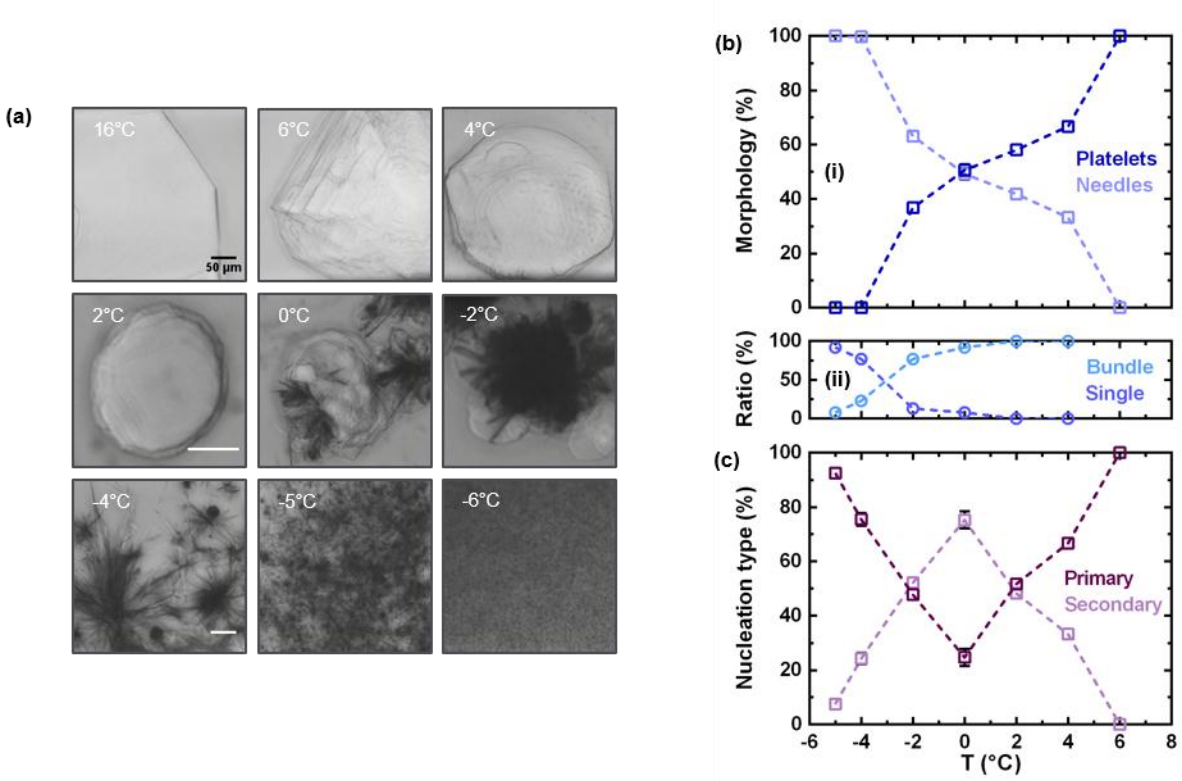

Figure 8. Visual characterization of the morphologies and nucleation types after a cooling quench to a range of temperatures. (a) Optical microscopy images of the predominant crystal habit; between 2 and -2 ºC all three habits shown are prevalent with varying proportion. (b)(i) Morphology assignment, broadly classified as platelets and needles. (ii) Further categorization of the needle morphology as bundles and single needles. (c) Nucleation type was termed as primary if nucleation was isolated, or secondary if development ensued from another crystal.

Crystallization is slow at the highest temperatures (>4 °C), generally yielding octagonal platelets, whose development can be termed 'continuous' as the sides grow proportionally.[17] As the temperature is lowered, the platelets become increasingly rounded. Two mechanisms are generally thought to underpin crystal growth: volume-diffusion and surface-integration controlled.[23] With the experiments conducted the solution is stationary, therefore it is predicted that growth is predominantly volume-diffusion controlled.[23,33,54] Adsorption onto a planar crystal face, however, is expected to incur a large energy penalty,[21] especially when related to the commencement of a new layer. It is thus anticipated that platelet crystal growth is influenced

by a combination of the two processes. Based on the optical microscopy images, spiral growth can be clearly observed on the flat (F) faces of the platelets at 4 and 6 °C, shown in Figure 2(b). These faces are the slowest growing and are thus morphologically most important. Two-dimensional nucleation and growth, caused by the adsorption, diffusion and agglomeration on a crystal F face, is observed around 2 °C where supersaturation is higher, shown in Figure 2(c). It is anticipated that rough growth occurs at the lowest temperatures (≤0 °C).[16,35,65] The platelet sides, considered to be either kinked (K) or stepped (S) faces, proceed via a rough growth mechanism at all temperatures.

At low temperatures, crystallization rates are higher and faces develop at different rates, illustrated in Supporting Information (Figure S6), giving rise to underdeveloped or absent sides;[21] their evolution is thus described as structural.[17] This is reflected in the morphology, with an increased proportion of needles, which grow rapidly in two-directions, as shown in Figure 8(b)(i). Fast growth rates are likely to introduce defects, lowering the attachment energy onto the faces;[21] growth is therefore expected be mainly volume-diffusion controlled.[23] Under these conditions, rough growth appears to occur on all faces. The proportion of needles to platelets increases gradually with decreasing temperature, as estimated in Figure 8(b)(i).

Crystal nucleation was classified as primary or secondary, according to whether an isolated nucleation event was observed, or whether crystallization ensued from an existing crystal respectively.[29] The results are shown in Figure 8(c), with a detailed example in Supporting Information (Figure S9(b)) for the -5 °C solutions. At 6 °C primary nucleation occurs because nucleation rates are extremely low and the faces grow with relatively minimal imperfections, resulting in a low probability of contact nucleation occurring (shear nucleation is unlikely as the solution is stationary).[22] As the temperature is decreased $\Delta t_{(N)}$ increases, displayed in Figure 4(d), and the crystalline sides are less smooth, hence contact (secondary) nucleation increases,[21] reaching a maximum by 0 °C. Below 0 °C the decrease in secondary nucleation is attributed to $\Delta t_{(N)}$ decreasing; by -5 °C primary nucleation and growth appear to be fast enough to mostly reach completion before secondary nucleation events occur.

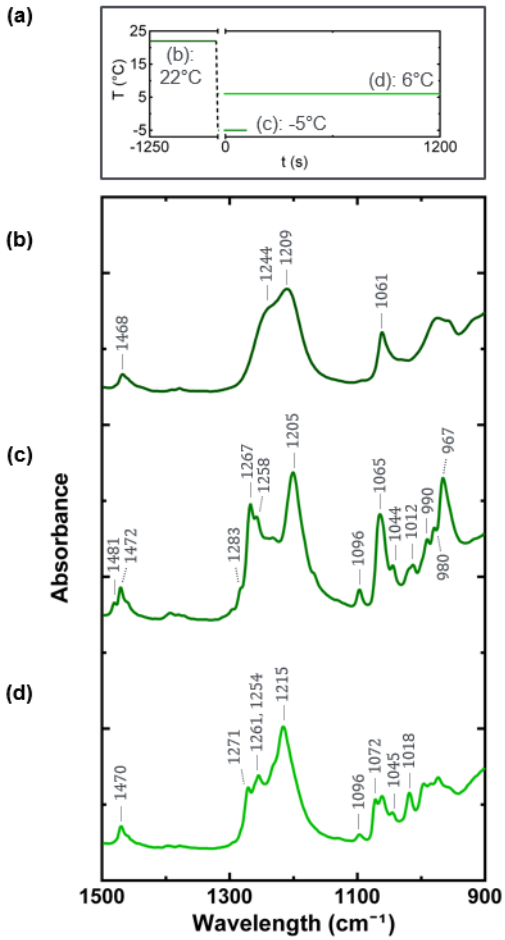

Figure 9. ATR-FTIR spectra to characterize the hydration states of the morphologies observed via optical microscopy. (a) Temperature profiles for spectra (b) to (d). (b) 20% SDS-H_2O micellar solution, conducted as a reference point. (c) Hydrated crystals from rapid cooling to -5 °C. (d) Hydrated crystals from rapid cooling to 6 °C.

FTIR spectra of SDS crystals[44] and their hydration states has been reported,[45] therefore this technique was employed to relate the hydration states to the morphologies observed via optical microscopy. Equilibrium phase mapping of SDS-H_2O indicated that the *equilibrium* crystal form for the micellar solutions investigated is the dihydrate, SDS·$2H_2O$.[12] In addition, several non-equilibrium forms have been observed, specifically the ⅛, mono- and hemihydrates, depending on the cooling rate and temperature.[45,46]

In the current work, solutions of platelets and needles were obtained by rapid (50 °C min^{-1}) cooling to 6 and -5 °C respectively. The micellar solution at 22 °C was also measured as a reference. The spectra from 1500 to 900 cm^{-1} are given in Figures 9(b) to (d), with the full spectra provided in the Supporting Information (Figure S10). As the methyl stretching bands for the micellar and crystalline forms are comparable; the majority of the structural determination is based on the stated wavelength range.[45] The structure of the needles was assigned to the hemihydrate, based on the reported spectrum.[45] Octagonal platelets have previously been observed during linear heating and cooling studies of SDS-H_2O and were classified as the ⅛ hydrate using computer simulations.[46] However, conflicting reports suggest that ⅛ hydrates are only formed via solvent evaporation (for instance using $CHCl_3$:MeOH (9:1, v:v))[37] or at very high (>90%) SDS-H_2O concentrations.[12] Our measurements clearly indicate that the structure is the monohydrate; platelets are thus associated with this crystal form.

The dominant crystal forms are thus the hemihydrate, with a molar ratio of SDS·½H_2O and the monohydrate, SDS·1H_2O. Evidently in the micellar solutions considered, containing 10 to 30% SDS-H_2O, a large excess of water does not take part in the crystallization process. A 20% SDS-H_2O solution, for instance, has a molar ratio of approximately 1:64. The above crystal size estimations, shown in Figure 5(d), assume that the crystallized volume is 100%. To investigate whether H_2O crystals coexist with the hydrated SDS crystals, a series of control experiments with H_2O, 0.2% SDS-H_2O (<cmc)[66] and 2% SDS-H_2O were carried out, shown in Supporting Information (Figure S11). Within the relevant temperature and timescales of the above experiments, no crystallization was observed. The crystalline morphologies must thus comprise a suspension of hydrated SDS crystals in an excess of water, not captured by the projected area microscopy imaging.

CONCLUSION

The crystallization processes for the ubiquitous binary surfactant system, SDS-H_2O, in the micellar composition range was studied under isothermal conditions between 20 and -6 °C. Time resolved microscopy

and calorimetry enabled the quantification of relative nucleation and growth rates, in addition to relating the various habits observed to crystalline polymorphs using ATR-FTIR. Between 8 and 20 °C nucleation rates were exceptionally low, with virtually no nuclei forming within 6 h. Growth, however, occurred within this temperature range if seed crystals generated at lower temperatures were used, with the rate of growth decreasing exponentially with increasing temperature. The fastest nucleation and growth rates, and correspondingly the shortest induction times were found below -4 °C, where quantitative experimentation becomes challenging as the crystallization and thermal equilibration timescales become commensurate.

Two characteristic crystal morphologies were observed: platelets and needles (either as bundles or single needles), found to dominate from high to low temperatures. Using ATR-FTIR, needles and platelets were associated with the hemihydrate and monohydrate polymorphs respectively. For micellar concentrations of SDS below the crystallization phase boundary, these are distinct from the equilibrium crystalline hydration state, the dihydrate, which forms upon interconversion of the above forms. The crystallization kinetics were well-described by the Avrami equation, with dimensionality $n \approx 2.3$ and an activation energy of ≈ 218 kJ mol^{-1}. Overall, our results enable the predictive design of SDS crystal habits with a well-defined density, size distribution, morphology and polymorph under non-equilibrium conditions.

ASSOCIATED CONTENT

Supporting information

Experimental details for NMR (and spectra) and the image analysis procedure; additional nucleation, crystallization kinetics and morphology data; and full DSC and ATR-FTIR spectra. This material is available free of charge via the Internet at http://pubs.acs.org.

AUTHOR INFORMATION

Corresponding Author

*E-mail: j.cabral@imperial.ac.uk

Author contributions

The manuscript was written through contributions of all authors. All authors have given approval to the final version of the manuscript.

Notes

The authors declare no competing financial interest.

Acknowledgements

We thank the Engineering and Physical Sciences Research Council (EPSRC), the Institute of Chemical Biology and Procter & Gamble for a PhD studentship for RMM. JC thanks EPSRC for financial support EP/L020564/1. We are grateful to Dr Andrew J. P. White for useful discussions on crystallography, Dr Alessandra Vitale for assistance with ATR-FTIR measurements and Ms Patricia Carry for use of the DSC.

REFERENCES

(1) Chappat, M. *Colloids Surf., A.* **1994**, *91*, 57–77.

(2) Hargreaves, A. E. *Chemical Formulation: An Overview of Surfactant-Based Preparations Used in Everyday Life*; Royal Society of Chemistry: Cambridge, U.K., 2003.

(3) Rosen, M. J. *Surfactants and Interfacial Phenomena*, 3rd ed.; John Wiley: New Jersey, 2004; pp 208–242.

(4) Doe, P. H.; El-Emary, M.; Wade, W. H.; Schecter, R. S. *J. Am. Oil Chem. Soc*. **1977**, *54*, 570–577.

(5) Thompson, L. *J. Colloid Interface Sci.* **1994**, *163*, 61–73.

(6) Smulders, E.; von Rybinsk, W.; Nordskog, A. *Ulmann's Encyclopedia of Industrial Chemistry*; Wiley-VCH: Weinham, 2011; pp 355–450.

(7) Jafari, S. M.; Assadpoor, E.; He, Y.; Bhandari, B. *Food Hydrocolloids* **2008**, *22*, 1191–1202.

(8) Bibette, J.; Calderon, F. L.; Poulin, P. *Rep. Prog. Phys.* **1999**, *62*, 969–1033.

(9) Mason, T. G.; Bibette, J. *Langmuir* **1997**, *13*, 4600–4613.

(10) Wibowo, C.; Ng, K. M. *AIChE J.* **2001**, *47*, 2746–2767.

(11) Schägger, H. *Nat. Protoc.* **2006**, *1*, 16–22.

(12) Kékicheff, P.; Grabielle-Madelmont, C.; Ollivon, M. *J. Colloid Interface Sci.* **1989**, *131*, 112–132.

(13) Kékicheff, P. *J. Colloid Interface Sci.* **1989**, *131*, 133–152.

(14) Fontell, K. *Mol. Cryst. Liq. Cryst.* **1981**, *63*, 59–82.

(15) Lacmann, R.; Herden, A.; Mayer, C. *Chem. Eng. Technol.* **1999**, *22*, 279–289.

(16) Lovette, M. A.; Browning, A. R.; Griffin, D. W.; Sizemore, J. P.; Snyder, R. C.; Doherty, M. F. *Ind. Eng. Chem. Res.* **2008**, *47*, 9812–9833.

(17) Zhang, Y.; Sizemore, J. P.; Doherty, M. F. *AIChE J.* **20-06**, *52*, 1906–1915.

(18) Kind, M. *Chem. Eng. Process* **1999**, *38*, 405–410.

(19) Lechuga-Ballesteros, D.; Rodríguez-Hornedo, N. *Int. J. Pharm.* **1995**, *115*, 151–160.

(20) Van Hook, A. *Crystallization: Theory and Practice*; Reinhold Pub. Corp.: New York, 1961; pp 1–153.

(21) Sunagawa, I. *Crystals: Growth, Morphology and Perfection*; Cambridge University Press: Cambridge, 2005; pp 10–155.

(22) Garside, J.; Mersmann, A.; Nyvlt, J. *Measurement of Crystal Growth and Nucleation Rates*, 2nd ed.; Institution of Chemical Engineers: Rugby, 2002.

(23) Rodríguez-Hornedo, N.; Murphy, D. *J. Pharm. Sci.* **1999**, *88*, 651–660.

(24) Vekilov, P.G. *Cryst. Growth Des.* **2010**, *10*, 5007–5019.

(25) Melia, T. P.; Moffitt, W. P. *J. Colloid Interface Sci.* **1964**, *19*, 443–447.

(26) Bigg, E. K. *Proc. Phys. Soc., Sect. B* **1953**, *66*, 688–694.

(27) Weissbuch, I.; Popovitz-Biro, R.; Lahav, M.; Leiserovitz, L. *Acta Crystallogr.* **1995**, *B51*, 115–148.

(28) Tadros, T. F. *Int. J. Cosmet. Sci.* **1992**, *14*, 93–111.

(29) Pamplin, B. R. *Crystal Growth*; Pergamon Press: Oxford, 1975.

(30) Bethell, D.; Fessey, R. E.; Namwindwa, E.; Roberts, D. W. *J. Chem. Soc., Perkin Trans. 2* **2001**, 1489–1495.

(31) Muramatsu, M.; Inoue, M. *J. Colloid Interface Sci.*, **1976**, *55*, 80–84.

(32) Dreger, E. E.; Keim, G. I.; Miles, G. T.; Sedlowsky, L.; Ross, J. *Ind. Eng. Chem.* **1944**, *36*, 610–617.

(33) Mangin, D.; Puel, F.; Veesler, S. *Org. Process. Res. Dev.* **2009**, *13*, 1241–1253.

(34) Bernstein, J.; Davey, R. J.; Henck, J.- O. *Angew. Chem., Int. Ed.* **1999**, *38*, 3440–3461.

(35) Snyder, R. C.; Doherty, M. F. *AIChE J.* **2007**, *53*, 1337–1348.

(36) Chemburkar, S. R.; Bauer, J.; Deming, K.; Spiwek, H.; Patel, K.; Morris, J.; Henry, R.; Spanton, S.; Dziki, W.; Porter, W.; Quick, J.; Bauer, P.; Donaubauer, J.; Narayanan, B. A.; Soldani, M.; Riley, D.; McFarland, K. *Org. Process Res. Dev.* **2000**, *4*, 413–417.

(37) Sundell, S. *Acta Chem. Scand.* **1977**, *A31*, 799–807.

(38) Coiro, V. M.; Mazza, F.; Pochetti, G. *Acta Crystallogr.* **1986**, *C42*, 991–995.

(39) Coiro, V. M.; Manigrasso, M.; Mazza, F.; Pochetti, G. *Acta Crystallogr.* **1987**, *C43*, 850–854.

(40) Smith, L. A.; Hammond, R. B.; Roberts, K. J.; Machin, D.; McLeod, G. *J. Mol. Struct.* **2000**, *554*, 173–182.

(41) Rawlings, F. F. J.; Lingafelter, E. C. *J. Am. Chem. Soc.* **1950**, *72*, 1852.

(42) Rawlings, F. F. J.; Lingafelter, E. C. *J. Am. Chem. Soc.* **1955**, *77*, 870-872.

(43) Picquart, M. *J. Phys. Chem.* **1986**, *90*, 243–250.

(44) Thompson, W. K. *Spectrochim. Acta*, **1974**, *30A*, 117–124.

(45) Sperline, R. P. *Langmuir* **1997**, *13*, 3715–3726.

(46) Smith, L. A.; Duncan, A.; Thomson, G. B.; Roberts, K. J.; Machin, D.; McLeod, G. *J. Cryst. Growth* **2004**, *263*, 480–490.

(47) Smith, L. A.; Roberts, K. J.; Machin, D.; McLeod, G. *J. Cryst. Growth* **2001**, *226*, 158–167.

(48) Smith, L. A.; Thomson, G. B.; Roberts, K. J.; Machin, D.; McLeod, G. *Cryst. Growth Des.* **2005**, *5*, 2164–2172.

(49) Mossop, S. C. *Proc. Phys. Soc., Sect. B* **1954**, *68*, 193–208.

(50) Avrami, M. *J. Chem. Phys.* **1939**, *7*, 1103–1112.

(51) Rozwadowski, T.; Massalska-Arodź, M.; Kolek, Ł.; Grzybowska, K.; Bąk, A.; Chłędowska, K. *Cryst. Growth Des.* **2015**, *15*, 2891–2900.

(52) Cosgrove, T. *Colloid Science: Principles, Methods and Applications*, 2nd ed.; Wiley: Bristol, U.K., 2010; pp 61–90.

(53) Kashchiev, D. *Nucleation: Basic Theory with Applications*; Butterworth-Heinemann: Oxford, U.K., 2000; pp 371–390.

(54) Erdemir, D.; Lee, A. Y.; Myerson, A. S. *Acc. Chem. Res.* **2009**, *42*, 621–629.

(55) Hurle, D. T. J.; *Handbook of Crystal Growth, 1a. Fundamentals. Thermodynamics and Kinetics*; Elsevier: North-Holland, Amsterdam, 1993; pp 249–306.

(56) Supaphol, P.; Spruiell, J. E. *Polymer* **2001**, *42*, 699–712.

(57) Mo, Z.; Wang, S.; *Eur. Polym. J.* **1997**, *33*, 1405–1414.

(58) Liu, S. Y.; Yu, Y. N.; Cui, Y.; Zhang, H. F.; Mo, Z. *J. Appl. Polym. Sci.* **1988**, *70*, 2371–2380.

(59) Avrami, M. *J. Chem. Phys*. **1940**, *8*, 212–224.

(60) Avrami, M. *J. Chem. Phys*. **1941**, *9*, 188–184.

(61) Lorenzo, A. T.; Arnal, M. L.; Albuerne, J.; Müller, A. *J. Polym. Test.* **2007**, *26*, 222–231.

(62) Schick, C. *Anal. Bioanal. Chem.* **2009**, *395*, 1589–1611.

(63) Marangoni, A. G. *J. Am. Oil Chem. Soc.* **1998**, *75*, 1465–1467.

(64) Cebe, P.; Hong, S.-D. *Polymer* **1986**, *27*, 1183–1192.

(65) Hartman, P.; Perdok, W. G. *Acta Crystallogr.* **1955**, *8*, 49–52.

(66) Mukerjee, P.; Mysels, K. J. *Critical Micelle Concentrations of Aqueous Surfactant Systems*; NSRDS-NBS 36; U. S. Department of Commerce: Washington, DC, 1971.

For Table of Contents Use Only

Isothermal Crystallization Kinetics of Sodium Dodecyl Sulfate–Water Micellar Solutions

Ruhina M. Miller[†,‡], Andreas S. Poulos[‡], Eric S. J. Robles[§], Nicholas J. Brooks[†], Oscar Ces[†], João T. Cabral*[‡]

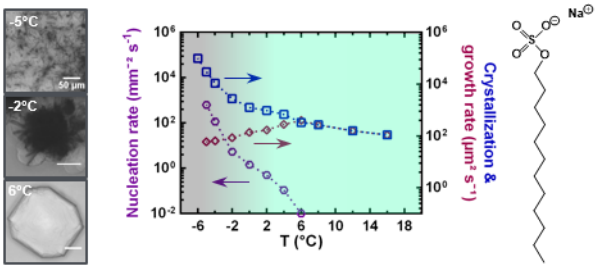

Kinetic and morphological insight into the crystallization of micellar SDS-H_2O solutions under isothermal conditions, using a combination of optical microscopy, differential scanning calorimetry and attenuated total reflection Fourier transform infrared spectroscopy.